Chapter 20

Hydraulic and Sleeve Fracturing Laboratory Experiments on 6 Rock Types

Sebastian Brenne, Michael Molenda, Ferdinand Stöckhert and Michael Alber

Additional information is available at the end of the chapter

http://dx.doi.org/10.5772/56301

1. Introduction

Hydraulic tensile strength is a crucial value for planning reservoir stimulation and stress measurements. It is used in the classical breakdown pressure (P_b) relation by Hubbert & Willis [1], where P_b is a function of major and minor principal horizontal stresses S_H and S_h, hydraulic tensile strength σ_T and pore pressure P_0:

$$P_b = 3S_h - S_H + \sigma_T - P_0 \tag{1}$$

For hydraulic fracturing laboratory experiments (MiniFrac – MF) under isostatic confining pressure P_m this might be reduced to:

$$P_b = cP_m + \sigma_T - P_0 \tag{2}$$

The coefficient c should be equal to two when porepressure is neglected. However, many laboratory experiments [2,3] resulted in values of about 1 for c, which might be explained by poroelastic effects.

Thus, when poroelasticity is excluded in the experiments by taking dry samples and sealing off the central borehole by an impermeable membrane (like a polymer tube), one would expect that c equals two and σ_T will be in the range of the tensile strength as determined by other tensile strength tests.

However, experiments with jacketed boreholes (sleeve MiniFrac – SMF) yield remarkable high values for c (about 6 to 8) and also for σ_T (about 3 to 5 times the tensile strength of the material) [4]. As a consequence we use a linear elastic fracture mechanics approach to evaluate our experiments.

1.1. Theory of hydraulic and sleeve fracturing on hollow cylinders

Fracture mechanics deal with stress concentrations around fractures and the definition of propagation criteria for fractures. The theory is essentially based on the works of Griffith [5] and Irwin [6], which led to the introduction of the stress intensity factor K.

$$K = \sigma\sqrt{\pi a} \tag{3}$$

K represents the magnitude of the elastic stress singularity at the tip of a fracture of the length $2a$ subjected to a uniform stress σ. With this concept, it is possible to formulate a simple fracture propagation criterion $K = K_C$. The fracture propagates when K reaches a critical value K_C (fracture toughness) with the fracture toughness assumed to be a property of the rock.

Mode I stress intensity factors (K_I) for arbitrary tractions $(\sigma(x))$ applied to the surface of a fracture of the length $2a$ may be computed by following formula [7,8]:

$$K_I = \frac{1}{\pi\sqrt{a}} \int_{-a}^{a} \sigma(x) \left(\frac{a+x}{a-x} \right)^{\frac{1}{2}} dx \tag{4}$$

The direction of propagation is the x-axis and the stresses are applied perpendicular to the fracture. As can be seen from equation (4), K_I increases with growing fracture length. A simple, 2-dimensional model was assumed for determination of stress intensity factors at the crack tips of the hydraulically induced fractures in MF and SMF tests.

Two fractures of length a are radially emanating from a circular hole of radius r in an infinite plate subjected to a compressive far field stress of the magnitude P_m. A fluid pressure P_{inj} is acting on the borehole wall and the pressure inside the fractures is either zero (SMF) or equal to the pressure in the borehole (MF: $P_{frac} = P_{inj}$). Stress intensities on the fracture tips can be determined by superposition of stress intensity factors resulting from each loading type [2,3]:

$$K_{I-MF} = K_I(P_m) + K_I(P_{inj}) + K_I(P_{frac}) \tag{5}$$

$$K_{I-SMF} = K_I(P_m) + K_I(P_{inj}) \tag{6}$$

http://dx.doi.org/10.5772/56301

$K_{I-MF/SMF}$ are not only dependent on the fracture length a (cf. Equations (3) and (4)) but also on the borehole radius r (see Appendix).

K_{I-MF} (full pressure in the fracture) gives an upper bound for stress intensities in this geometry (actual K_I_MF might be lower due to a negative pressure gradient inside the fracture), while K_{I-SMF} is only induced by the pressure in the borehole and far-field stresses and is therefore substantially lower than K_{I-SMF} (Figure 1).

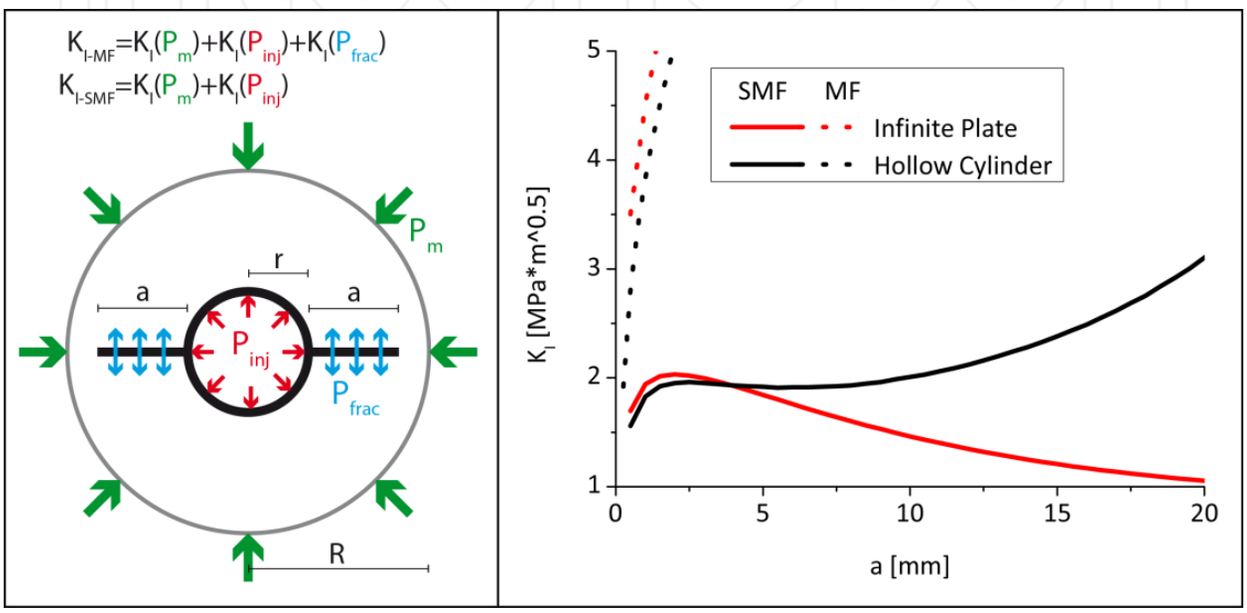

Figure 1. Left side: superposition of stress intensities by each loading type. Right side: stress intensity factor versus fracture length from analytical (infinite plate) and numerical (hollow cylinder) calculations for $r = 3$ mm, $P_{inj} = 50$MPa, $P_m = 0$ and an outer radius R of the hollow cylinder = 30 mm.

As an analytical solution for $K_I(P_m)$ and $K_I(P_{inj})$ for the ring geometry (corresponding to the hollow cylinder) is quite complex, we used the simpler solutions for a circular hole in an infinite plate as described by Rummel and Winter [2,3] (cf. Appendix). We compared the results of numerical simulations for the ring geometry with analytical solutions for the infinite plate. These results indicate that the simplification might be valid for fracture lengths smaller then $a \approx \frac{R-r}{10}$ with $R = 10r$ (R is the outer radius of the ring geometry (cf. Figure 1).

Solving K_{I-MF} and K_{I-SMF} for P_{inj} and setting $K_{I-MF} = K_{I-SMF} = K_{IC}$ (mode I fracture toughness) yields a critical injection pressure $(P_C(a))$ for each crack length a. If P_{inj} reaches $P_C\ (a)$, the fracture will propagate. From Figure 2 it can be seen, that $P_C\ (a)$ is very large for very small crack lengths. In consequence, the presence of microcracks is required for the formation of macroscopic fractures.

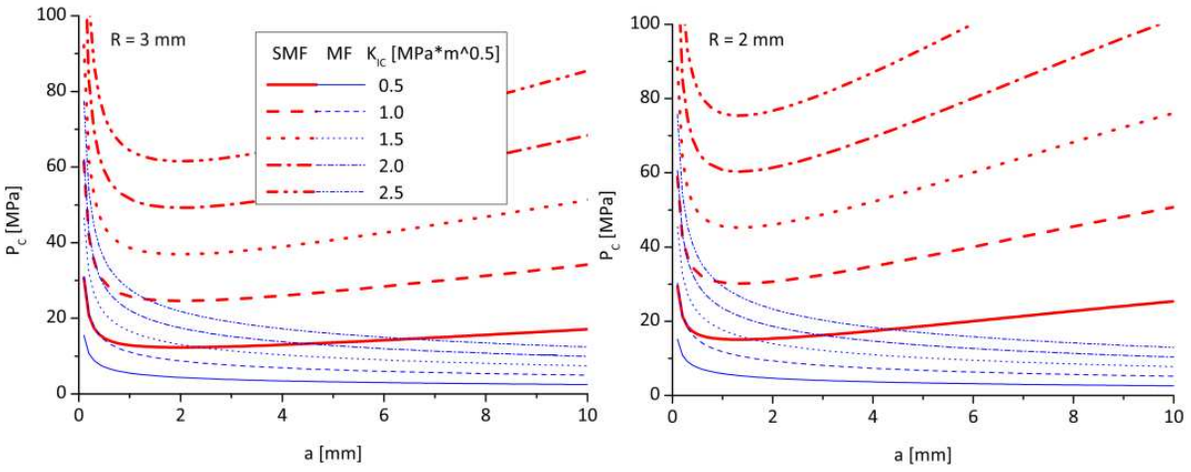

Figure 2. Critical injection pressure for fracture propagation P_C depending on fracture length a for $P_m = 0$. Borehole radii $r = 3$ mm (left), $r = 2$mm (right).

MF-equation (Equation 13) with full injection pressure in the fracture yields unstable fracture propagation at constant injection pressures as soon as microcracks start to propagate. On the other hand, the SMF-equations (Equation 14) show a minimum. Thus, after a fracture reaches the crack length corresponding to the minimum critical injection pressure, stable fracture propagation (i.e. to propagate the fracture, the injection pressure has to be increased) could be expected.

To calculate the coefficient c from Equation 2, we assume the presence of microcracks of a fixed length a_0 in the sample. The corresponding $P_C(a_0)$ versus P_m for the MF case (pressure in fracture = injection pressure) yields a coefficient $c = 1$, which is independent of a_0. $P_C(a_0)$ while for SMF the c value depends strongly on the assumed microcrack length a_0 and gives $c > 2$ (increasing a_0 yield higher c).

2. Sample preparation and rock testing

The core specimens are drilled either with 40 mm or 62 mm water cooled diamond core drills. Core end planes are cut with a water flushed diamond saw blade and ground coplanar to a maximum deviation of ± 0.02 mm. The length and diameter ratio is chosen between 1.5:1 and 2.25:1. After sample preparation core specimens were dried for two days at a temperature of 105°C. For calculations of porosity Φ, measurements of bulk density ρ_d and of grain density ρ_s via pycnometer were done. Static geomechanical parameters

http://dx.doi.org/10.5772/56301

were determined by uniaxial and triaxial compressive as well as Brazilian disc tensile strength test series according to ISRM and DGGT suggested methods [9,10]. Mode I fracture toughness was determined using the Chevron notched three-point bending test according to [9]. Furthermore, a dynamic rock parameter, the compressional ultra-sonic wave velocity (v_p) was measured. For MF/SMF specimens a central axial borehole was drilled into cores, using a water flushed diamond hollow drill with an outer diameter of 4 mm or 6 mm.

rock type	era & period	quarry localization	Microstructure
marble	Triassic Upper	Carrara Italy	coarse monocrystalline polygonal fabric
limestone	Jurassic upper Malm	Treuchtlingen South Germany	micritic limestone with abundant fossils and stylolites
sandstone	Carboniferous Mississippian	Dortmund/Hagen West Germany	fine-grained arcose
andesite D	Permian Rotliegend	Doenstedt N German Basin	porphyric fine-grained partly altered and pre-fractured
rhyolite	Permian Rotliegend	Flechtingen N German Basin	porphyric fine-grained partly pre-fractured and sealed joints
andesite R	Permian Rotliegend	Thuringian Forest Rotkopf	porphyric coarse-grained and pre-fractured

Table 1. Rock types used in our experiments.

2.1. Stress field and injection

Figure 3 shows schematically the components of the MF and SMF experimental set-up. The stress field is induced by a hydraulic ram (capacity 4500 kN) through a servo controlled MTS Test Star II system with a Hoek triaxial cell which is pressurized using a hand pump to achieve simultaneous pressure increase of confining pressure and axial load. In all tests axial stress is set to be 2.5 MPa higher than P_m to prevent leakage. Distilled water is pumped into borehole as the injection fluid (MF) or into a polymer tube inside the borehole (SMF). A servo controlled pressure intensifier with a maximum injection pressure of 105 MPa was used to perform a constant pumping rate of 0.1 ml/s. With this apparatus also steady-state flow tests were conducted to obtain rock permeability values (according to the procedure described in [11]).

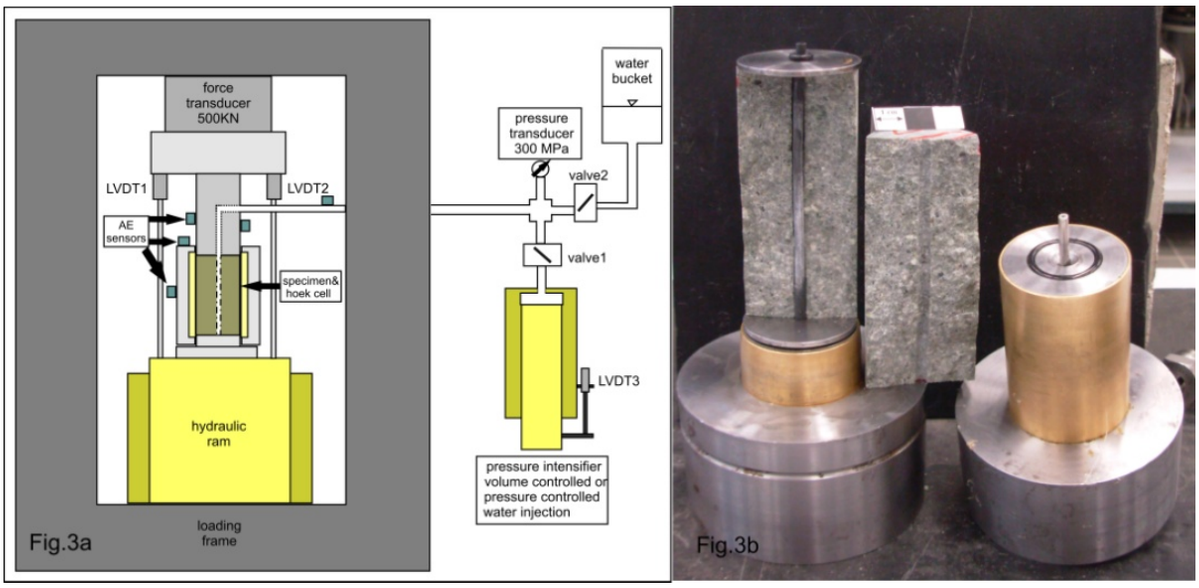

Figure 3. (a) Sketch of MF experimental set up including AE monitoring sensors (not shown are the pressure transducer and hand pump system to regulate confining pressure in the Hoek cell). (b) Typical specimen after SMF experiment.

2.2. Acoustic emission monitoring

Acoustic Emission (AE) signals are acquired with an AMSY5 Acoustic Emission Measurement System (Vallen Systeme GmbH, Germany) equipped with 5 Sensors of type VS150-M. The VS150-M Sensors operate over a frequency range of 100-450 kHz with a resonance frequency at 150 kHz. Due to machine noise in the range below 100 kHz incoming signals are filtered by a digital bandpass-filter that passes a frequency range of 95-850 kHz. AE data are sampled with a sampling rate of 10 MHz. The sensors are fixed using hot-melt adhesive to ensure best coupling characteristics. Pencil-break tests (Hsu-Nielsen source [12]) and sensor pulsing runs (active acoustic emission by one sensor) are used to test the actual sensor coupling on the sample.

3. Results

3.1. Petrophysical and mechanical parameters

An overview of the rock properties is given in Table 2. A wide range of low porosity/permeability rocks with K_{IC} from 1 to 2 MPa $\cdot\sqrt{m}$ were tested.

rock type	ρ_d [g/cm³]	Φ [-]	k [m²]	v_p [m/s]	KIC [MPa · √m]	C/φ [MPa]/[°]	E_{stat} [GPa]	σ_T [MPa]
marble	2.71 ±0.002	0.40 ±0.08	1E-19	5.67 ±0.06	1.57 ±0.11 (N=3)	29/22	36.0 ±1.0	6.4 ± 1.5
limestone	2.56 ±0.008	5.64 ±0.04	1E-18	5.59 ±0.05	1.19 ±0.14 (N=8)	27/53	32.2 ±1.6	8.2 ± 2.2
sandstone	2.57 ±0.006	4.39 ±0.06	8E-18	4.61 ±0.13	1.54 ±0.13 (N=4)	36/50	29.4 ±1.6	13.2 ± 2.1
rhyolite	2.63 ±0.015	1.02 ±0.12	9E-19	5.39 ±0.34	2.16 ±0.10 (N=4)	20…36/55	30.2 ±1.9	15.8 ± 3.2
andesite D	2.72 ±0.023	0.51 ±0.09	6E-19	5.26 ±0.28	1.90 ±0.08 (N=2)	20…41/50	28.7 ±3.1	14.6 ± 4.5
andesite R	2.60 ±0.013	1.70 ±0.08	4E-20	4.35 ±0.27	1.63 ±0.24 (N=4)	31/46	21.3 ±0.9	11.4 ± 2.8

Table 2. Mean values and standard deviations of petrophysical and mechanical parameters of tested rocks: dry bulk density ρ_d, porosity Φ, permeability k, compressive wave velocity v_p, fracture toughness from Chevron notched three-point bending tests K_{IC}, cohesion C and friction angle φ from a Mohr-Coulomb fit, Young's modulus E_{stat}, σ_T as determined by Brazilian disc tensile strength tests.

3.2. MF and SMF experiments

A schematic example of typical experiment data for MF and SMF tests is shown in Figure 4. Acoustic emission recordings are used to identify fracture processes in the test specimens. AE counts (threshold crossings per time interval – corresponding to AE activity) can directly be linked to localized fracture propagation [4]. The pressure at which the AE count rate raises rapidly is defined as P_{AE}, which is further used as initial fracture propagation pressure. P_{AE} is picked where the AE count rate permanently exceeds 1/10 of the test's average (see Figure 4).

In MF experiments, there is almost no AE activity prior to failure. Failure occurs in a very short time span just before sample breakdown (which occurs at maximum injection pressure $P_{inj\ max} = P_b$), therefore in MF experiments $P_{AE} \approx P_b$. In contrast, SMF experiments show an exponential increase in AE activity at injection pressures that are substantially lower than the actual breakdown pressure ($P_{AE} < P_b$), but much higher than P_{AE} in MF experiments. Therefore, it is possible to interrupt the experiment after AE activity started but before sample breakdown. The latter occurs in SMF experiments when the sample is completely splitted into two parts, which results in a tube breakdown and therefore in an injection pressure drop. Thin sections of specimens, where the experiment was interrupted, show macroscopic fractures emanating several millimeters into the sample but without any connection to the outer surface.

Noteworthy is the discrepancy between the MF and SMF initial fracture propagation pressures P_{AE} at zero confining pressure. This result would imply different hydraulic tensile strength values for the same rock type when using equation (2). Furthermore there is a significant difference between the values of coefficient c calculated for MF and SMF experiments. This

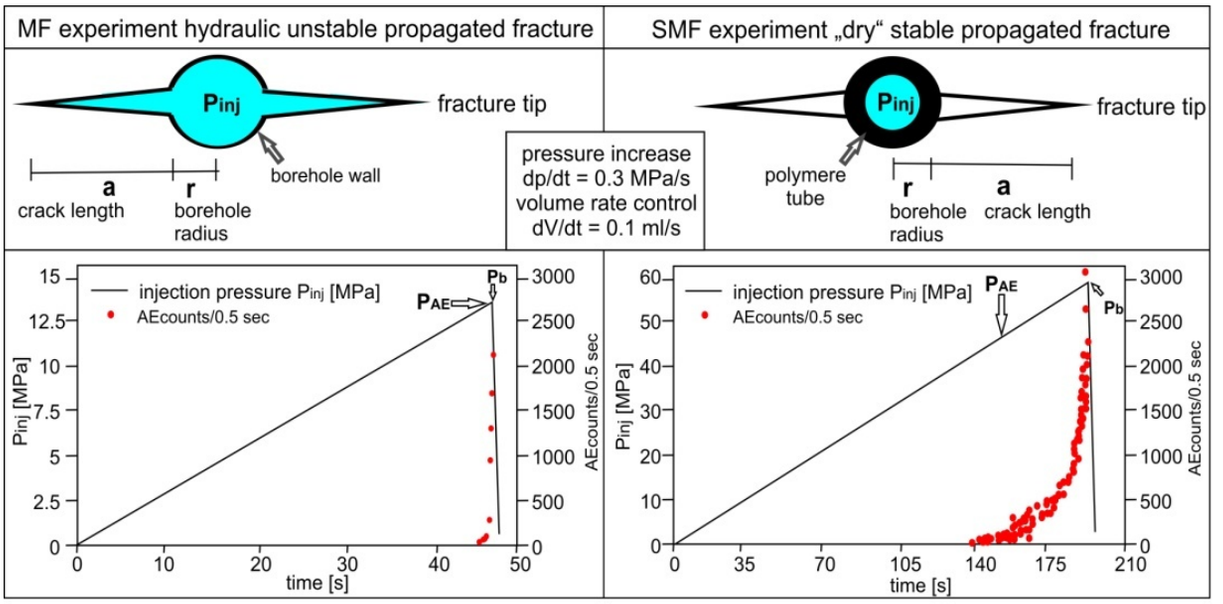

Figure 4. Schematic differences between MF (left) and SMF (right) experiments.

can be seen clearly in Figure 5. Scale effects in P_{AE} (Figure 2) with borehole radius are not evident for the 2 and 3 mm borehole radius samples due to data scattering. One single SMF test of a sandstone with a 6.35 mm borehole radius showed a significantly lower P_{AE} as can be seen in Figure 5.

			MF			SMF	
rock type	**Borehole diam.**	**N**	**PAE0 [MPa]**	***c***	**N**	**PAE0 [MPa]**	***c***
marble	4 mm	8	7.7	1.03	6	31.7	6.97
	6 mm	8	9.4	0.96	4	19.6	8.54
limestone	4 mm	9	10.3	1.00	6	26.7	6.06
	6 mm	8	8.2	1.01	7	29.1	5.79
sandstone	4 mm	8	18.2	1.13	5	41.7	6.29
	6 mm	8	18.5	1.14	4	40.5	7.26
rhyolite	4 mm	11	18.2	0.89	4	51.6	6.04
	6 mm	8	16.0	0.85	5	50.9	5.88
andesite D	4 mm	9	16.1	1.00	3	64.2	4.17
	6 mm	6	10.9	0.87	4	48.1	4.83
andesite R	4 mm	10	10.0	1.17	4	47.4	6.26
	6 mm	6	8.2	1.17	5	29.7	7.44
		∑ 93	-	Ø 1.02	∑ 57	-	Ø 6.33

Table 3. Results of all MF and SMF rock type test series in form of P_{AE0} and coefficient c (see equation (2)). N gives the number of tested samples per lithology and borehole diameter.

http://dx.doi.org/10.5772/56301

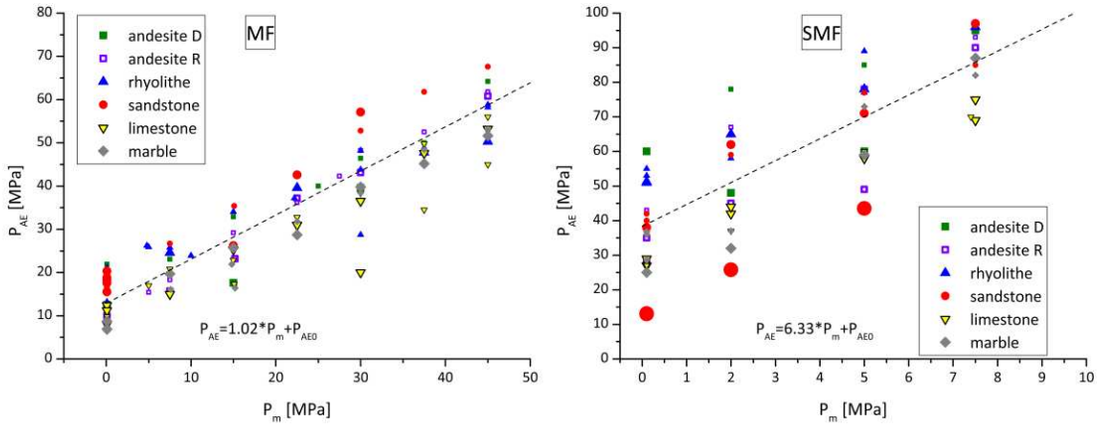

Figure 5. Experimental results of MF (left) and SMF (right) initial fracture propagation pressures for different confining pressures. Dashed line – linear regression of test data. Symbol size refers to borehole radius r (small – $r = 2mm$; intermediate – $r = 3mm$; large – $r = 6.35mm$)

4. Conclusion

With SMF tests, stable fracture propagation was achieved over a wide range of injection pressure. Fracture initiation can be confidently linked to the AE count rates. This can be concluded from experiments that were interrupted after P_{AE} but below breakdown pressure. Physical examination revealed the presence of distinct fractures in these specimens (see Figure 6).

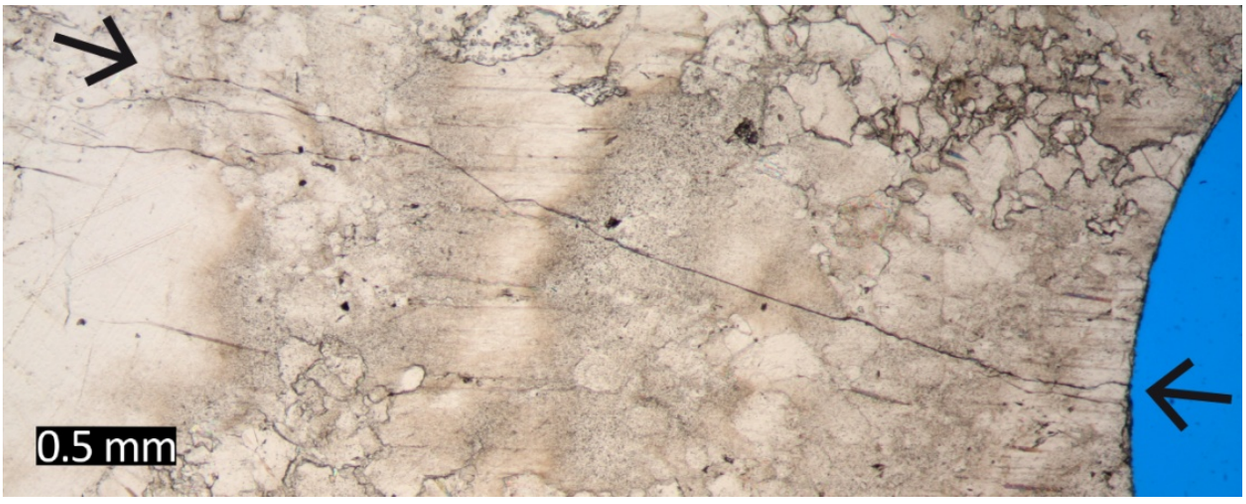

Figure 6. Thin-section of a marble specimen ($r = 2$mm) after SMF test. Clearly visible is a "dry" fracture (indicated by arrows) emanating radially from the borehole (at the right side of the picture). The experiment was interrupted before specimen breakdown. The fracture did apparently not propagate to the outer wall of the specimen.

Due to high data scatter, the theoretical scale effect (critical injection pressure P_c is higher for smaller borehole radii) cannot be resolved by our data. However, tests with a larger (r = 6.35 mm) borehole give some support to the notion.

The simple fracture mechanics model is able to explain the higher P_{AE} in SMF experiments. Equations 5 and 6 include the influence of fractures (with or without pressure inside), which is omitted in the classical approach (Equation 1). The high coefficient c in SMF test can only be explained by assuming high microcrack lengths ($a_0 \approx 6$ mm).

We excluded poroelastic effects in our analysis due to the use of initially dry rocks with low permeabilities.

Appendix

Superposition of stress intensity factors for two radial cracks of length a emanating from an internally pressurized (P_{inj}- injection pressure in the borehole, P_{frac}- pressure inside the fracture) circular hole of radius r in an infinite plate subjected to an isostatic far-field stress P_m as described by [2] and [3] :

$$K_I\left(P_m\right) = P_m\sqrt{r} * f_{Pm}\left(a,r\right) \tag{7}$$

$$K_I\left(P_{inj}\right) = P_{inj}\sqrt{r} * f_{P_{inj}}\left(a,r\right) \tag{8}$$

$$K_I\left(P_{frac}\right) = P_{frac}\sqrt{r} * f_{P_{frac}}\left(a,r\right) \tag{9}$$

$$f_{Pm}\left(a,r\right) = 2\left(1+\frac{a}{r}\right)^2\left(\frac{\left(1+\frac{a}{r}\right)^2-1}{\left(\pi\left(1+\frac{a}{r}\right)\right)^7}\right)^{\frac{1}{2}} + \left(\pi\left(1+\frac{a}{r}\right)\right)^{\frac{1}{2}}\left(1-\frac{2}{\pi}\sin^{-1}\left(\frac{1}{1+\frac{a}{r}}\right)\right) \tag{10}$$

$$f_{P_{inj}}\left(a,r\right) = \left(1.3\frac{\frac{a}{r}}{1+\left(1+\frac{a}{r}\right)^{\frac{3}{2}}} + \frac{7.8\left(\sin\left(\frac{2a}{r}\right)\right)}{2\left(1+\frac{a}{r}\right)^{\frac{5}{2}}-1.7}\right) \tag{11}$$

$$f_{P_{frac}}(a,r) = \left(\pi\left(1+\frac{a}{r}\right)\right)^{\frac{1}{2}}\left(1-\frac{2}{\pi}\sin^{-1}\left(\frac{1}{1+\frac{a}{r}}\right)\right) \tag{12}$$

Note: In equations 10 and 12 the borehole was excluded from the integration of stresses (cf. equation 4). The critical fracture propagation pressure at a given fracture length a, borehole radius r and mode I fracture toughness K_{IC} for the unjacketed (P_{c-MF}) and the jacketed (P_{c-SMF}) case:

$$P_{c-MF} = \frac{1}{f_{P_{inj}} * f_{P_{frac}}}\left(\frac{K_{IC}}{\sqrt{r}} + P_m f_{P_m}\right) \tag{13}$$

$$P_{c-SMF} = \frac{1}{f_{P_{inj}}}\left(\frac{K_{IC}}{\sqrt{r}} + P_m f_{P_m}\right) \tag{14}$$

Acknowledgements

The authors wish to thank the German Federal Ministry for the Environment, Nature Conservation and Nuclear Safety for financing our project (FKZ 0325279B). Many core specimens were prepared and analyzed by our student staff: T. Hoferichter, J. Braun, S. Hönig, K. Bartmann and A. Kraft. A great praise to the precision mechanics workshop guys for the construction of the fine working pressure intensifier system. We appreciate fruitful discussions with geomecon GmbH, Potsdam.

Author details

Sebastian Brenne*, Michael Molenda, Ferdinand Stöckhert and Michael Alber

*Address all correspondence to: sebastian.brenne@rub.de

Ruhr-University Bochum, Germany

References

[1] Hubbert M, Willis D. Mechanics of hydraulic fracturing. Petroleum Transactions. 1957;210:153–68.

[2] Rummel F. Fracture Mechanics Approach to Hydraulic Fracturing Stress Measurements. In: Atkinson BK, editor. Fracture mechanics of rock. Academic Press geology series. London [.u.a.]: Academic Pr; 1987. p. 217–39.

[3] Winter R. Bruchmechanische Gesteinsuntersuchungen mit dem Bezug zu hydraulischen Frac-Versuchen in Tiefbohrungen. Berichte des Instituts für Geophysik der Ruhr-Universität Bochum: Reihe A. Bochum; 1983.

[4] Ito T, Hayashi K. Physical background to the breakdown pressure in hydraulic fracturing tectonic stress measurements. International Journal of Rock Mechanics and Mining Sciences & Geomechanics Abstracts. 1991;28:285–93.

[5] Griffith AA. The Phenomena of Rupture and Flow in Solids. Philosophical Transactions of the Royal Society of London. Series A, Containing Papers of a Mathematical or Physical Character. 1921;221:163–98.

[6] Irwin GR. Analysis of stresses and strains near the end of a crack traversing a plate. Journal of Applied Mechanics. 1957;24:361–64.

[7] Sih GC. Handbook of stress-intensity factors: Stress-intensity factor solutions and formulars for reference. Bethlehem, Pa: Lehigh Univ., Inst. of Fracture and Solid Mechanics; 1973.

[8] Tada H, Paris PC, Irwin GR. The stress analysis of cracks handbook. 3rd ed. New York: ASME Press; 2000.Ulusaihutsen

[9] Ulusay R, Hudson JA, editors. The complete ISRM suggested methods for rock characterization, testing and monitoring: 1974-2006. 2007th ed. Ankara: Commission on Testing Methods, International Society of Rock Mechanics; 2007.

[10] Mutschler T. Neufassung der Empfehlung Nr. 1 des Arbeitskreises "Versuchstechnik Fels" der Deutschen Gesellschaft für Geotechnik e. V.: Einaxiale Druckversuche an zylindrischen Gesteinsprüfkörpern. Bautechnik. 2004;81:825–34.

[11] Selvadurai APS, Jenner L. Radial Flow Permeability Testing of an Argillaceous Limestone. Ground Water. 2013;51:100–07.

[12] ASTM E976. Standard guide for determining the reproducibility of acoustic emsission sensor response. American Society for Testing and Materials. 1994;386-391.